A novel nonlocal reduction-based coupling approach via Arlequin method on instability patterns

Fan Xu, Salim Belouettar, Heng Hu, Michel Potier-Ferry

CSMA 2013
11e Colloque National en Calcul des Structures
13-17 Mai 2013

A novel nonlocal reduction-based coupling approach via Arlequin method on instability patterns

Fan XU [1,2,*], Salim BELOUETTAR [2], Heng HU [3], Michel POTIER-FERRY [1]

[1] LEM3, UMR CNRS 7239, Université de Lorraine, France, fan.xu@univ-lorraine.fr, michel.potier-ferry@univ-lorraine.fr
[2] CRP Henri Tudor, Luxembourg, fan.xu@tudor.lu, salim.belouettar@tudor.lu
[3] School of Civil Engineering, Wuhan University, P.R. China, huheng@whu.edu.cn
[*] Corresponding author

Résumé — A Fourier-related nonlocal reduction-based coupling, using the bridging domain methodology, is investigated to analyze the influence of boundary conditions on wrinkling patterns. The nonlocal reduction-based coupling approach is based on the well-known Arlequin framework. The analysis of the effect of boundary conditions on instability patterns is then provided. Numerical evaluation of the nonlocal reduction-based coupling approach is proposed by considering the case of buckling of a long beam lying on a nonlinear elastic foundation.
Mots clés — Buckling, Arlequin method, Multi-scale, Nonlocal, Boundary effect, Fourier transform.

1 Introduction

A new approach based on the concept of Fourier series with slowly varying coefficients has been presented recently, which is developed to study the instabilities with nearly periodic patterns [1, 2, 3]. The mathematical representation yields to generalized continua macroscopic models. In this technique, the macroscopic field is defined by Fourier coefficients of the microscopic field. It has been established that the models obtained in this way are consistent with the Landau−Ginzburg technique, but they may remain also valid beyond the bifurcation point, and the coupling between global and local instabilities can be taken into consideration. Besides, this approach could be very useful to analyze the instability problems like Rayleigh−Bénard convection whose discretization requires a huge number of degrees of freedom. Nevertheless, a clear and secure boundary condition cannot be introduced into these macroscopic models, which is a drawback intrinsically linked to the use of any model reduction.

To solve this problem, a multi-scale modeling approach has been proposed in order to bypass the question of boundary conditions [4] : the full model is implemented near the boundary while the envelope model is considered elsewhere, and these two models are bridged by the Arlequin method [5]. In order to match two types of displacement in two models, for simplicity, it carried out a natural prolongation coupling way, which means the coupling is based on the fine model. However, according to the Arlequin framework [6, 7], coupling based on the coarse model is preferred to avoid the locking phenomena.

The present paper proposes to methodically answer these shortcomings. For this purpose, a novel nonlocal reduction-based coupling approach is developed, implemented and evaluated. In this context, the Arlequin method is adopted in order to couple the microscopic fine model and the macroscopic envelope model. In the proposed approach, the Fourier coefficients are computed through reduction over a period. This constitutes a very original contribution that aims at developing a nonlocal coupling approach so as to accurately describe the boundary behaviour and completely avoid the locking phenomena in terms of both amplitude and phase.

2 Macroscopic modelling of instability pattern formation

As in paper [3], the multi-scale approach, based on the concept of Fourier series with slowly varying coefficients, is adopted in the present paper. Let us consider a physical phenomenon described by the field $U(x)(x \in \mathbb{R})$. The instability wave number q is known. The unknowns of the model $U =$

$\{u(x), v(x), n(x)...\}$ are described as Fourier series, whose coefficients vary more slowly than the harmonics :

$$U(x) = \sum_{j=-\infty}^{+\infty} U_j(x) e^{jiqx}, \tag{1}$$

where the Fourier coefficient $U_j(x)$ denotes the envelope for the j^{th} order harmonic and $U_{-j}(x)$ denotes its conjugate value. The macroscopic unknown fields $U_j(x)$ slowly vary over a period $\left[x, x+\frac{2\pi}{jq}\right]$ of

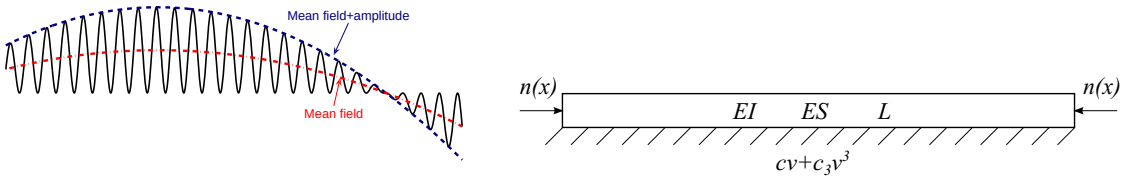

Fig. 1 – The left shows at least two macroscopic fields (the mean field and the amplitude of the fluctuation) are necessary to describe a nearly periodic response. The right is sketch of an elastic beam on a nonlinear elastic foundation.

the oscillation. It is worth to mention that at least two functions, $U_0(x)$ and $U_1(x)$, are necessary to describe the nearly periodic patterns as depicted in Fig. 1. $U_0(x)$ is identified as the mean value and $U_1(x)$ represents the envelope or the amplitude of the spatial oscillations. Notice that $U_0(x)$ is real valued and $U_1(x)$ can be expressed as $U_1(x) = r(x)e^{i\varphi(x)}$. The latter mathematical expression represents the first harmonic where $r(x)$ is the amplitude modulation and $\varphi(x)$ is the phase modulation. The main idea of macroscopic modelling is to deduce some differential equations satisfied by the amplitude $U_j(x)$.

In what follows, an elastic beam, resting on a nonlinear elastic foundation is used for the development of the microscopic model (see Fig. 1). The unknowns are the components $u(x)$ and $v(x)$ of the displacement vector and the normal force $n(x)$. So $U(x) = \{u(x), v(x), n(x)\}$ and the analyzed problem is described by the following set of differential equations :

$$\begin{cases} \dfrac{dn}{dx} + f = 0, & (a) \\ \dfrac{n}{ES} = \dfrac{du}{dx} + \dfrac{1}{2}\left(\dfrac{dv}{dx}\right)^2, & (b) \\ \dfrac{d^2}{dx^2}\left(EI\dfrac{d^2v}{dx^2}\right) - \dfrac{d}{dx}(n\dfrac{dv}{dx}) + cv + c_3v^3 = 0. & (c) \end{cases} \tag{2}$$

These equations are referred to as the microscopic model. The periodic patterns are fully described by four structural parameters : EI, ES, c, c_3 and an axial force $f(x)$. Note that the solutions of the system (2) are the stationary points of the following potential energy :

$$P(u,v) = \int_0^L \left(\frac{ES}{2}(u' + \frac{v'^2}{2})^2 + \frac{EI}{2}v''^2 + \frac{c}{2}v^2 + \frac{c_3}{4}v^4 - fu\right) dx. \tag{3}$$

In paper [3], many simplifications have been introduced to build the simplest macroscopic model that can couple the membrane problem with the envelope equation similar to Landau−Ginzburg equation. Finally, the simplified potential energy of macroscopic model is given by

$$P(u_0, v_1) = \int_0^L \left(\frac{ES}{2}\left(u_0' + v_1'^2 + q^2v_1^2\right)^2 + EI\left(6q^2v_1'^2 + q^4v_1^2\right) + cv_1^2 + \frac{3c_3}{2}v_1^4 - f_0u_0\right) dx. \tag{4}$$

The differential equations of the system follow from the stationary behaviour of the potential energy $\delta P = 0$. This leads to

$$\begin{cases} \dfrac{dn_0}{dx} + f_0 = 0, & (a) \\ n_0 = ES(u_0' + v_1'^2 + q^2v_1^2), & (b) \\ -\dfrac{d}{dx}\left[(6EIq^2 + n_0)\dfrac{dv_1}{dx}\right] + \left(EIq^4 + n_0q^2 + c\right)v_1 + 3c_3v_1^3 = 0. & (c) \end{cases} \tag{5}$$

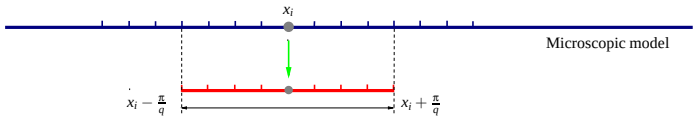

Fig. 2 – Schematic of the reduction of microscopic model.

It is not easy to associate consistent boundary conditions with macroscopic models like (4) and (5). Indeed, the assumption of slowly varying oscillation is not valid everywhere, especially near the boundary due to the presence of boundary layers [8]. The very simplified model (4) and (5) is able to predict the amplitude modulation, but unable to predict the phase modulation.

3 Reduction from micro behaviour to Fourier coefficients

Although the approach of using slowly variable Fourier coefficients is well established [1, 2, 3], how to obtain the envelopes from given micro behaviour $(U(x) \rightarrow U_j(x))$ is still challenging. This issue will be addressed from the mathematical standpoint to the finite element point of view. Moreover, the methodology of the nonlocal reduction will be applied in the reduction-based coupling approach in the next section.

For a periodic function $U(x)$ that is integrable on $\left[-\frac{\pi}{q}, \frac{\pi}{q}\right]$, the Fourier coefficients can be represented as

$$U_j = \frac{q}{2\pi} \int_{-\frac{\pi}{q}}^{\frac{\pi}{q}} U(x) e^{-jiqx} dx. \tag{6}$$

Using Euler's formula, U_j can be divided into a real part U_j^R and an imaginary part U_j^I.

From the mathematical standpoint, it is straightforward to obtain all the envelopes through Eq. (6). From the finite element method perspective, the real microscopic model (2) and (3) is used to assess the nonlocal reduction. The reduction of the transversal displacement is conducted by considering five envelopes. A clamped beam is defined with the following parameters : $L = 30\pi$, $ES = 1$, $EI = 1$, $c = 1$ and $c_3 = 1/3$. The instability wave number is taken as $q = 1$. In this configuration, the beam is free of body forces and subjected to an increasing global end shortening $u(L) = -\lambda L$. The beam is meshed using 120 microscopic elements with the element length $l_e = \pi/4$. Basically, any point of the discretized beam can be used to implement the proposed nonlocal reduction. The only exception is the points on boundary region $\left[0, \frac{\pi}{q}\right]$ and $\left[L - \frac{\pi}{q}, L\right]$, since the numerical integration is carried out over the period $\left[-\frac{\pi}{q}, \frac{\pi}{q}\right]$. For the sake of simplicity, each node of the element is considered as the center of the numerical integration. Therefore, each reduction point covers eight elements over the whole period as depicted in Fig. 2.

The discretization of the nonlocal reduction can be written as

$$U_j^R = \frac{q}{2\pi} \int_{x_i - \frac{\pi}{q}}^{x_i + \frac{\pi}{q}} U(x) \cos(jqx) dx = \frac{q}{2\pi} \frac{l_e}{2} \sum_{x_n \in gp} U(x_n) \cos(jqx_n), \tag{7}$$

$$U_j^I = -\frac{q}{2\pi} \int_{x_i - \frac{\pi}{q}}^{x_i + \frac{\pi}{q}} U(x) \sin(jqx) dx = -\frac{q}{2\pi} \frac{l_e}{2} \sum_{x_n \in gp} U(x_n) \sin(jqx_n), \tag{8}$$

where x_i is the node of element. $x_n \in gp$ represents the corresponding Gauss point on the microscopic elements within the integration domain $\left[x_i - \frac{\pi}{q}, x_i + \frac{\pi}{q}\right]$.

The reduction of the transverse displacement v is performed with Hermite shape functions. The variations, over the domain $[\pi, 29\pi]$, of five different envelopes : v_0, v_1^R, v_1^I, v_2^R and v_2^I, are depicted in Fig. 3. It can be observed that $|v_1^I|$ and $|v_1^R|$ are much larger than the other three envelopes. In the meanwhile, the median values of v_0, v_2^R and v_2^I are all close to zero. In addition, when substituting the values of envelopes v_1^I and v_1^R in Eq. 6 to construct the microscopic behaviour v(x), it can be noticed that only these two envelopes can sufficiently cover the microscopic model as shown in Fig. 4. Actually, in this case, only five envelopes have been assumed. Theoretically, the microscopic transversal displacement can be exactly illustrated if the number of envelope is infinite, yet it is not necessary and practical.

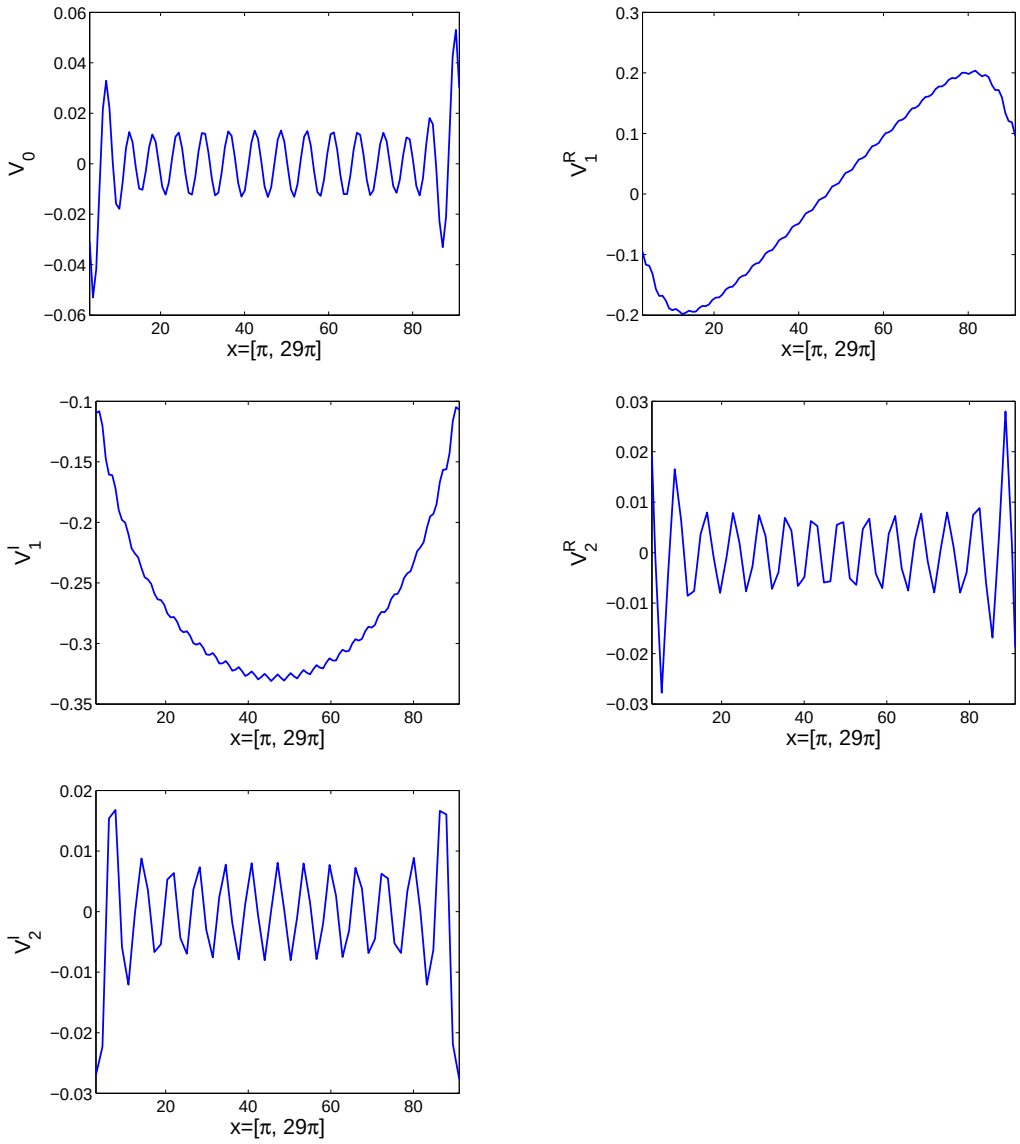

Fig. 3 – One real envelope (v_0) and four complex envelopes (v_1^R, v_1^I, v_2^R, v_2^I). The reduction is performed over the domain $[\pi, 29\pi]$. The instability pattern of $\lambda = 2.21$.

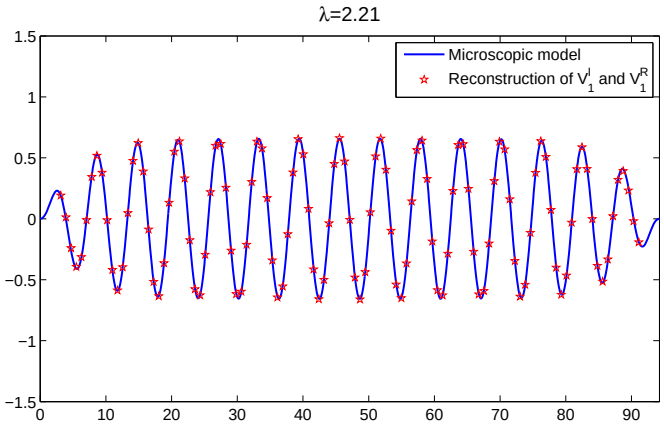

Fig. 4 – Buckling of a clamped beam under uniform compression. The instability pattern of $\lambda = 2.21$. The length of beam is 30π. The reconstruction of reduced Fourier coefficients v_1^I and v_1^R is over the domain $[\pi, 29\pi]$.

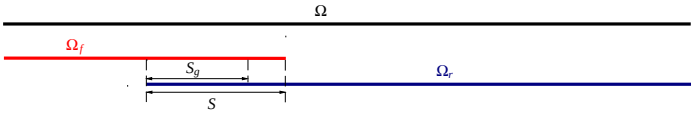

Fig. 5 – Definition of domains in the Arlequin framework.

4 Arlequin method in the context of nonlocal coupling

The microscopic model (2) and (3) is implemented in a small region close to the boundary. This allows introducing the "exact" boundary conditions. The simplified envelope model (4) and (5) will be applied in the bulk. The two models can be bridged together thanks to the Arlequin framework [5, 6].

The domain Ω, representing the whole mechanical system, is partitioned into two overlapping subzones : Ω_f (microscopic fine model domain) and Ω_r (macroscopic reduced model domain). The resulting superposition zone $S = \Omega_f \cap \Omega_r$ contains the gluing zone $S_g \subseteq S$ (see Fig. 5).

Defining $\boldsymbol{u}_f = \{u(x), v(x) : x \in \Omega_f\}$ and $\boldsymbol{u}_r = \{u_0(x), v_1(x) : x \in \Omega_r\}$, the energy contribution of the two models is defined as

$$\begin{cases} P_f(\boldsymbol{u}_f) = \displaystyle\int_{\Omega_f} [\alpha_f W(\boldsymbol{u}_f) - \beta_f f u]\, d\Omega, \\ P_r(\boldsymbol{u}_r) = \displaystyle\int_{\Omega_r} [\alpha_r W(\boldsymbol{u}_r) - \beta_r f_0 u_0]\, d\Omega, \end{cases} \tag{9}$$

in which

$$\begin{cases} W(\boldsymbol{u}_f) = \dfrac{ES}{2}(u' + \dfrac{v'^2}{2})^2 + \dfrac{EI}{2}v''^2 + \dfrac{c}{2}v^2 + \dfrac{c_3}{4}v^4, \\ W(\boldsymbol{u}_r) = \dfrac{ES}{2}(u_0' + v_1'^2 + q^2 v_1^2)^2 + EI(6q^2 v_1'^2 + q^4 v_1^2) + c v_1^2 + \dfrac{3c_3}{2}v_1^4. \end{cases} \tag{10}$$

The energy associated to each domain is balanced by weight parameter functions which are represented by α_i for the internal work and β_i for the external work. More details on selection of these functions can be found in [6, 7]. In this work, a linear weight function is considered in the overlapping region.

4.1 Coupling alternatives

The coupling aims at connecting the microscopic model with envelope model. According to the Arlequin framework, generally, coupling based on the coarse model is preferred to avoid the locking phenomena. This requires a definition of a nonlocal reduction operator $\boldsymbol{u}_f \to \mathfrak{R}(\boldsymbol{u}_f)$ which involves the Fourier transform. Contrarily, the other way is to perform the inverse connection by using a local prolongation operator $\boldsymbol{u}_r \to \mathfrak{P}(\boldsymbol{u}_r)$, which reproduces a compatible field from $\boldsymbol{u}_r$ to be coupled with $\boldsymbol{u}_f$. Therefore, the coupling is conducted by requiring that one of the two following conditions to be satisfied in a mean sense :

$$\mathfrak{R}(\boldsymbol{u}_f) - \boldsymbol{u}_r = 0, \quad \forall x \in S_g; \tag{11}$$

$$\boldsymbol{u}_f - \mathfrak{P}(\boldsymbol{u}_r) = 0, \quad \forall x \in S_g. \tag{12}$$

Due to the nonlocal character of the proposed Fourier transform in nonlocal reduction-based coupling approach, the implementation of (11) is much more intricate. The analysis and numerical implementation of the nonlocal reduction-based coupling approach will be detailed in the next sections, while the details of the prolongation coupling approach (12) can be found in [4].

4.2 Reduction-based coupling approach

For transversal direction, the reduction operator is the Fourier coefficient which has the nonlocal character over a period. Based on the discussion reported in Section 2, one can deduce the relation among v_1^R, v_1^I and $r(x)$ as follows :

$$v(x) = v_1(x)e^{iqx} + v_{-1}(x)e^{-iqx} = \left(v_1^R + iv_1^I\right)e^{iqx} + \left(v_{-1}^R + iv_{-1}^I\right)e^{-iqx} = 2v_1^R\cos(qx) - 2v_1^I\sin(qx), \tag{13}$$

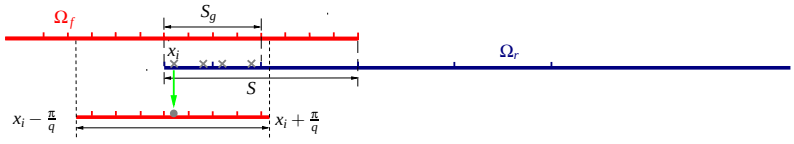

Fig. 6 – Schematic of the nonlocal reduction-based coupling approach. Two Gauss points are located at each macroscopic element in S_g.

where $v_{-1}^R = v_1^R$, $v_{-1}^I = -v_1^I$. After some algebraic manipulations, one can obtain

$$\begin{cases} r(x)\cos\varphi = v_1^R, \\ r(x)\sin\varphi = v_1^I. \end{cases} \tag{14}$$

Hence, the spatial evolution of the phase is described as $\varphi = \arctan\left(\frac{v_1^I}{v_1^R}\right)$. Considering the simplified envelope model (4), we choose $\varphi = -\pi/2$. Consequently,

$$\begin{cases} r(x) = -v_1^I, \\ v(x) = 2r(x)\sin(qx). \end{cases} \tag{15}$$

Therefore, only one envelope v_1^I is considered for the reduction. Consequently, the nonlocal reduction operator becomes

$$\mathfrak{R}_v(x_i) = \frac{q}{2\pi}\int_{x_i-\frac{\pi}{q}}^{x_i+\frac{\pi}{q}} v(x)\sin(qx)dx = \frac{q}{2\pi}\frac{l_e^j}{2}\sum_{x_j\in gp} v(x_j)\sin(qx_j), \tag{16}$$

where x_i is the Gauss point on the macroscopic element in S_g. $x_j \in gp$ represents the corresponding Gauss point on the microscopic element of length l_e^j within the integration region $\left[x_i - \frac{\pi}{q}, x_i + \frac{\pi}{q}\right]$.

It is worth to mention that the performed reduction is comparable to the one developed in Section 3. Here the Gauss point is the center of the numerical integration and the reduction is conducted at each Gauss point. This choice is motivated by the higher degree of accuracy when estimating $\boldsymbol{u}_r$ which accounts for the weak form of (11) as

$$\mathcal{C}(\boldsymbol{\lambda}, \mathfrak{R}(\boldsymbol{u}_f) - \boldsymbol{u}_r) = 0, \quad \forall \boldsymbol{\lambda} \in M, \quad \forall x \in S_g. \tag{17}$$

where $\boldsymbol{\lambda}$ is Lagrange multiplier as a fictive gluing force and M is the mediator space.

Notice that there are two main challenges when performing the numerical implementation. Indeed, the position of Gauss point is not located at the node of the element. Thus, the numerical integration of (16), over a period, might mismatch the corresponding position of the microscopic elements. Consequently, the bounds of the numerical integration will not match the positions of the nodes. In addition, the numerical integration, performed at Gauss points in the gluing zone S_g, may overlap in some regions. Furthermore, the bounds of the numerical integration, over the domain S_g, might lap either the domain S or the domain Ω_f. To cope with these numerical difficulties, the domain S is required to be a little larger than the domain S_g (see Fig. 6).

The corresponding stationary function is a Lagrange multiplier :

$$\mathcal{L}(\boldsymbol{u}_f, \boldsymbol{u}_r, \boldsymbol{\lambda}) = P_f(\boldsymbol{u}_f) + P_r(\boldsymbol{u}_r) + \mathcal{C}(\boldsymbol{\lambda}, \mathfrak{R}(\boldsymbol{u}_f) - \boldsymbol{u}_r). \tag{18}$$

From Eq. (18), one can obtain three equations according to $\delta\boldsymbol{u}_f$, $\delta\boldsymbol{u}_r$ and $\delta\boldsymbol{\lambda}$:

$$\begin{cases} \delta P_f(\boldsymbol{u}_f) + \mathcal{C}(\boldsymbol{\lambda}, \delta\mathfrak{R}(\boldsymbol{u}_f)) = 0, \quad \forall \delta\boldsymbol{u}_f \in K.A., \\ \delta P_r(\boldsymbol{u}_r) - \mathcal{C}(\boldsymbol{\lambda}, \delta\boldsymbol{u}_r) = 0, \quad \forall \delta\boldsymbol{u}_r \in K.A., \\ \mathcal{C}(\delta\boldsymbol{\lambda}, \mathfrak{R}(\boldsymbol{u}_f)) - \mathcal{C}(\delta\boldsymbol{\lambda}, \boldsymbol{u}_r) = 0, \quad \forall \delta\boldsymbol{\lambda} \in M. \end{cases} \tag{19}$$

where *K.A.* stands for kinematically admissible. Finally, the L^2 type coupling operator $\mathcal{C}$ is defined as follows :

$$\mathcal{C}(\boldsymbol{\lambda}, \boldsymbol{u}) = \int_{S_g} (\boldsymbol{\lambda}\cdot\boldsymbol{u})\, d\Omega. \tag{20}$$

More details about coupling operators can be found in [6, 7].

5 Numerical evaluation

Numerical evaluation of the nonlocal reduction-based coupling approach is performed by considering the case of buckling of a long beam lying on a nonlinear elastic foundation. The clamped beam has the same parameters as those reported in Section 3. Two models (microscopic model and macroscopic model) and two coupling approaches (reduction-based coupling and prolongation coupling [4]) are compared and evaluated.

As for reduction-based coupling approach, the bifurcation path (v_{max}, λ) and the instability pattern for $\lambda = 2.21$ are depicted in Fig. 7. As for prolongation coupling approach [4], the bifurcation branch (v_{max}, λ) and the instability pattern for $\lambda = 2.21$ are illustrated in Fig. 8.

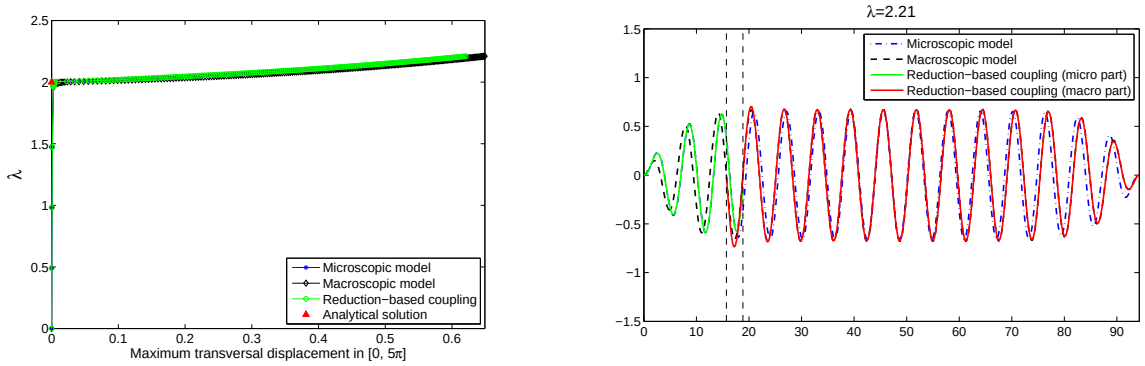

Fig. 7 – Buckling of a clamped beam under uniform compression : the left shows applied shortening λ vs. maximal deflection ; the right shows spatial distribution of the instability patterns for $\lambda = 2.21$. The reduction-based coupling approach is implemented.

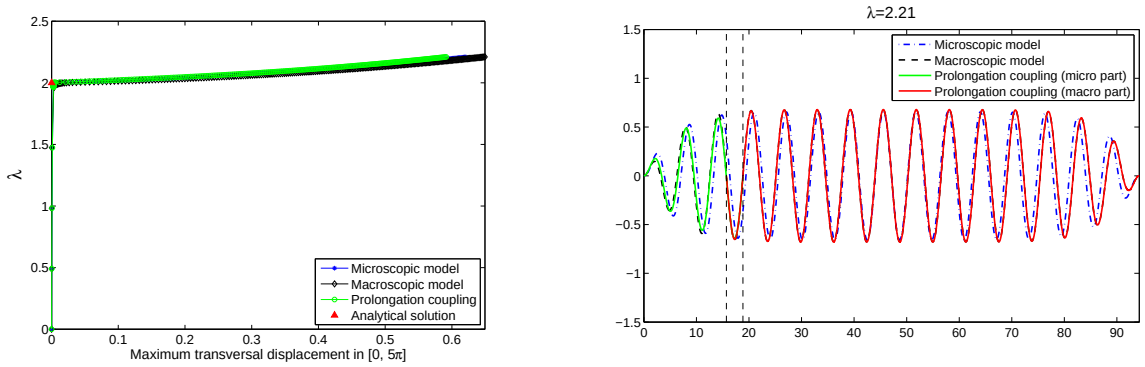

Fig. 8 – Buckling of a clamped beam under uniform compression : the left shows applied shortening λ vs. maximal deflection ; the right shows spatial distribution of the instability patterns for $\lambda = 2.21$. The prolongation coupling approach is implemented.

The following conclusions and remarks can be highlighted :

1. Regarding to the evolution of instability patterns, a disagreement between the macroscopic and microscopic model is observed. This is essentially due to the boundary effects that become significant at some distances from the bifurcation point. The macroscopic model is unable to describe boundary layers.
2. The reduction-based coupling approach is able to perfectly capture the local effects in the left boundary layers as depicted in Fig. 7 and 9. Precisely, there is no difference, in terms of amplitude or phase, between the reduction-based coupling approach and the microscopic model in the left part. This conclusion is consistent since the use of the microscopic model near the boundary accounts for the boundary layers. The proposed reduction-based coupling approach is able to correct the deficiency of the macroscopic model near the boundary.
3. According to the results reported in Fig. 8 and 9, the prolongation coupling approach [4] gives a fair result in terms of amplitude. However, there is a phase discrepancy in the left boundary

region due to the influence of phase locking phenomena when applying the prolongation coupling approach (see Fig. 9).

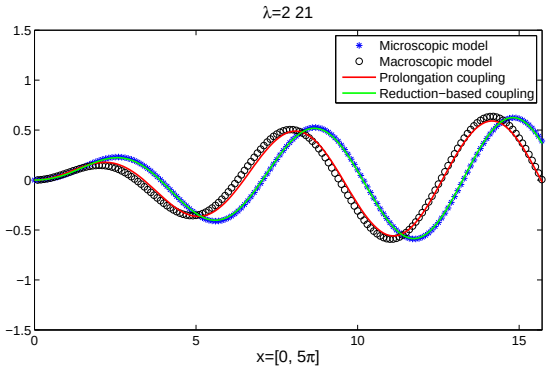

Fig. 9 – Zoom of the left boundary : spatial distribution of the instability patterns for $\lambda = 2.21$. The reduction-based coupling approach and prolongation coupling approach are depicted together.

6 Conclusion

In this paper, a nonlocal reduction-based coupling approach via Arlequin method has been developed to analyze the influence of boundary effects on pattern formation. In order to avoid the critical issue of defining appropriate boundary conditions for the macroscopic envelope model, the microscopic fine model has been introduced only in the vicinity of the boundary region. In this way, it allows prescribing the actual boundary conditions. The microscopic fine model and macroscopic envelope model are then bridged together through the proposed nonlocal reduction-based coupling approach. The reduction-based coupling approach is able to capture the local effects around the boundary layers and correct the deficiency of the macroscopic model. Our preliminary results show that this technique is promising and could be applied to cellular instability problems involving thin boundary layers such as membrane wrinkling and fiber microbuckling or even in fluid mechanics [8]. Besides, the reduction from microscopic behavior to Fourier coefficients has also raised some interests in deeply studying the number of harmonics to be accounted in macroscopic models [3] for various modelling cases.

Acknowledgement

The authors gratefully acknowledge the grant support by Fonds National de la Recherche Luxembourg (Grant No. : FNR/C10/MS/784868 − WRINKLE).

Références

[1] N. Damil, M. Potier-Ferry. *A generalized continuum approach to describe instability pattern formation by a multiple scale analysis*. Comptes Rendus Mécanique, 334 :674-678, 2006.

[2] N. Damil, M. Potier-Ferry. *A generalized continuum approach to predict local buckling patterns of thin structures*. European Journal of Computational Mechanics, 17 :945-956, 2008.

[3] N. Damil, M. Potier-Ferry. *Influence of local wrinkling on membrane behaviour : A new approach by the technique of slowly variable Fourier coefficients*. Journal of the Mechanics and Physics of Solids, 58(8) :1139-1153, 2010.

[4] H. Hu, N. Damil, M. Potier-Ferry. *A bridging technique to analyze the influence of boundary conditions on instability patterns*. Journal of Computational Physics, 230 :3753-3764, 2011.

[5] H. Ben Dhia. *Multiscale mechanical problems : the Arlequin method*. Comptes Rendus de l'Académie des Sciences, IIb(326) :899-904, 1998.

[6] H. Ben Dhia, G. Rateau. *The Arlequin method as a flexible engineering design tool*. International Journal for Numerical Methods in Engineering, 62 :1442-1462, 2005.

[7] P.T. Bauman, H. Ben Dhia, N. Elkhodja, J.T. Oden. *On the application of the Arlequin method to the coupling of particle and continuum models*. Computational Mechanics, 42 :511-530, 2008.

[8] H. Schlichting. *Boundary-Layer Theory*. 7th ed., McGraw-Hill, New York, 1979.